Structural Engineering and Mechanics, *Vol. 56, No. 6 (2015) 917-938*
DOI: http://dx.doi.org/10.12989/sem.2015.56.6.917

Quantitative impact response analysis of reinforced concrete beam using the Smoothed Particle Hydrodynamics (SPH) method

S.N. Mokhatar*[1], Y. Sonoda[2a], A.B.H. Kueh[3b] and Z.M. Jaini[3]

[1]Jamilus Research Center, Faculty of Civil and Environmental Engineering, University Tun Hussein Onn Malaysia, 86400, Batu Pahat, Johor, Malaysia
[2]Structural Analysis Laboratory, Department of Civil Engineering, Kyushu University, Motooka 744, Nishi-ku, Fukoka, Japan
[3]Construction Research Centre, Universiti Teknologi Malaysia, 81310 Skudai, Johor, Malaysia

(Received June 4, 2014, Revised August 10, 2015, Accepted November 5, 2015)

Abstract. The nonlinear numerical analysis of the impact response of reinforced concrete/mortar beam incorporated with the updated Lagrangian method, namely the Smoothed Particle Hydrodynamics (SPH) is carried out in this study. The analysis includes the simulation of the effects of high mass low velocity impact load falling on beam structures. Three material models to describe the localized failure of structural elements are: (1) linear pressure-sensitive yield criteria (Drucker-Prager type) in the pre-peak regime for the concrete/mortar meanwhile, the shear strain energy criterion (Von Mises) is applied for the steel reinforcement (2) nonlinear hardening law by means of modified linear Drucker-Prager envelope by employing the plane cap surface to simulate the irreversible plastic behavior of concrete/mortar (3) implementation of linear and nonlinear softening in tension and compression regions, respectively, to express the complex behavior of concrete material during short time loading condition. Validation upon existing experimental test results is conducted, from which the impact behavior of concrete beams are best described using the SPH model adopting an average velocity and erosion algorithm, where instability in terms of numerical fragmentation is reduced considerably.

Keywords: erosion; impact loading; modified Drucker-Prager; RC beam; smoothed particle hydrodynamics

1. Introduction

Reinforced concrete (RC) is one of the common materials that is extensively used as structural members in building constructions. When the impact load is applied to the RC beam, it will be deflected, at any instant, such that various forms of damages occur during the loading process. Under the impact loads, the RC beams may suffer from different types of global or localized

*Corresponding author, Ph.D., Email: shahruln@uthm.edu.my
[a]Professor, E-mail: sonoda@doc.kyushu-u.ac.jp
[b]Ph.D., E-mail: kbhahmad@utm.my

Copyright © 2015 Techno-Press, Ltd.
http://www.techno-press.org/?journal=sem&subpage=8 ISSN: 1225-4568 (Print), 1598-6217 (Online)

damage, including flexural cracking, shear cracking, crushing of concrete beneath the impactor and spalling at the bottom of the concrete element. Therefore, understanding the structural behavior, especially the beam element when subjected to impact loads is essential to protect this critical member from collapse, a direct result of an ultimate failure. It is common in engineering practice to conduct a series of experimental tests to determine a reliable set of impact properties of beam elements. The study of RC beams response under low velocity impact loads has been done experimentally by many researchers such as Kishi *et al.* (2003), Chen and May (2009), Fujikake *et al.* (2009), Saatci and Vecchio (2009), Sangi *et al.* (2010). However, estimating the response of RC structures under impact loading through full-scale tests is expensive in terms of providing the necessary test material, test equipment, and time to perform the procedure. Nowadays, the prediction of the response of impacted structures by implementing numerical analyses is starting to become more accurate and reliable. Combined with modern computer hardware and numerical hydrocodes, the computational time for such an assessment has been reduced to a satisfactory level. In presence of the developments of the computer program that is currently made in this field, the numerical models for the impact load assessment are fairly quick to obtain. Better understanding of each time step of the impact response phenomena can be investigated thoroughly by computational simulations.

Despite such aggressive progresses achieved in the computational field, it is worthwhile to note that analysis and design of structures that are focused on the dynamic loading are frequently very complex. Such analyses are further complicated when working with non-elastic materials such as RC. Thus, conventional structural analysis approach is not enough to define the real behavior of concrete element under severe load. Various grids or mesh methods such as finite element method (FEM), finite difference method (FDM) or finite volume method (FVM) have been explored for solving problems in the computational solid mechanics in particular those involve RC structures. As one of the most popular numerical methods, the FEM has been a greatly significant method and has achieved great success in various areas since its invention in 1950s. Over the past decades, the FEM has been widely employed for solving linear-elastic and elastic-plastic failure problems, as well as has become a common technique in civil engineering for predicting the response of structures and materials. Finite element (FE) is a general method of structural analysis, in which the solution for a problem in continuum mechanics is approximated by the analysis of an assemblage of FEs, which is interconnected at a finite number of nodal points that represents the solution to the problem.

One notable feature of the grid/mesh based numerical model is to divide a continuum domain into discrete small subdomains, via a process termed as discretization or meshing. The individual grid points (or nodes) are connected together in a pre-defined manner by a topological map, which is termed as a mesh (or grid). Despite their great success, some of the FE techniques have certain inherent advantages and disadvantages, which strictly depend on a large extent of its particular application. Some problems related to the use of mesh are the process of generating/regenerating a quality mesh and difficulties to assess the reliability calculation of shear failure, flexural failure and crushing phenomena of RC member. In the research papers of Charles (1987), Liu *et al.* (2006), Faham (2008), Ma *et al.* (2009), some weaknesses in the mesh-based numerical methods have been stated explicitly particularly when working on large deformation problems, which include crack propagation, free surface, deformable boundary, moving interface, complex geometry and mesh generation, mesh adaptivity, and multi-scale resolution.

2. Statement of the problem

A number of mathematical models dealing with the plastic constitutive law of concrete materials when subjected to various impact loads, such as collision and blast have been proposed in many technical papers (Park and Kim 2005, Rabczuk and Eibl 2006, Zhou *et al*. 2008, Gulkan and Korucu 2011, Gang *et al*. 2012, Youcai *et al*. 2013). However, the application of the precise constitutive model is very difficult due to their numerous and varying material parameters. Due to increase in the complexity of the model, the cost of the calculation may accordingly increase such that sometimes it is not efficiently useful for practical needs. In fact, the advanced existing plasticity models such as the Bresler-Pister model, William-Wranke model, Ottosen model, Reimann model and Hsieh-Ting-Chen model require many parameter identification that correspond to appropriate laboratory tests (tri-axial test, hydrostatic test, etc.). Thus, two-parameter simple models (like linear Drucker-Prager) are widely applied for practical use.

It has been recognized that many researchers (Saatci and Vecchio 2009, Unosson 2009, Kantar *et al.* 2011, Mokhatar and Abdullah *et al*. 2013) have successfully analyzed the elastic-plastic behavior of RC elements under low velocity impact loads using the FEM in simulating solid mechanics problem due to dynamic loads (impact, blast, etc.). However, their difficulties and limitations of FEM have been discussed extensively. One specific concern relates to the deformation of the material where the large relative movement of the connecting nodes cannot be tracked accurately if a fixed mesh is used. Thus, the employment of arbitrarily distributed particles without using any mesh is recommended to provide stable numerical solutions for such issue. For this particular matter, the Smoothed Particle Hydrodynamics (SPH) can be superior to the FEM to solve the limitation in the mesh-based technique. The SPH technique does not require a pre-defined mesh to render any connection of the particles during the process of computation. Besides, the SPH particles also carry material properties, and are allowed to move in light of the internal interactions and external forces.

During recent years, the application of mesh-less methods has been widely used for the evaluation of solid and structural behaviors in presence of the high-velocity impact (HVI) environment. Lavoie *et al.* (2015), Swaddiwudhipong *et al*. (2010), Ma (2009), Johnson (2011) have successfully applied SPH to study the perforation/penetration of aerospace structure, steel, thin plate and plain concrete subjected to HVI loads. Furthermore, typical bending failure problem of RC structural members under low impact velocity loads using SPH have also been presented in the study of Fukazawa and Sonoda (2011), Tokumaru *et al.* (2011), Mokhatar *et al.* (2013). These analyses employ the pressure independent criterion for concrete materials by ignoring the effect of confining pressure in the compression zone but considering only the tensile failure of the concrete.

The failure in compression region is more complex than that of tensile area since it is accompanied by lateral deformations. According to the presented literatures, the constitutive model concerned with the compressive behavior when subjected to low velocity impact loads by means of the SPH method is still as yet fully explored. In our effort to address these issues, we modified the linear Drucker-Prager (DP) yield line using a simple plane cap (PC) surface with lesser parameter identification incorporating the SPH to simulate the concrete plastic response. The aim is to simulate the compression volumetric change due to the outward and inward movements of the cap surface with the stress state such that the plane surface without the require of various parameters is used. This paper also presents the derivation of the proposed constitutive model and its softening technique to demonstrate the compression and tensile responses of concrete materials. It is assumed that all stress components at a point prior to the crushing are released entirely, and

the strength of the concrete is assumed to decrease completely. Then, the validation upon existing experimental test results is conducted, in which the concrete beams are described using the SPH model adopting an average velocity and erosion algorithm.

3. SPH method and numerical calculation setting

SPH technique is used in this study to examine its ability in the impact response analysis of the RC beam under low velocity collision. The procedure of SPH method uses a kernel interpolation to approximate the field variables at any particle in a support domain, *h*. The superscript *A* and *B* is used in this paper to denote the target particle *A* and neighboring particle *B*, respectively. For example, to calculate field variable such as the displacement, stress or strain of particle *A* in the domain integral, Ω, the integral of this particle is shown as

$$f(x^A) = \int_{\Omega} f(x^B) W^{AB}(x^A - x^B, h) dv^B \tag{1}$$

where $f(x^A)$ and $f(x^B)$ are functions of target particle *A* and neighboring particle *B*, respectively. Particle *A* is weighted by the kernel function, W^{AB} using a function of $W^{AB}(x^A - x^B, h)$, where, x^A and x^B are the positions of particles *A* and *B*, respectively. The integral computation in Eq. (1) is approximated by the summation of all neighboring particles *B* in the support domain, *h*.

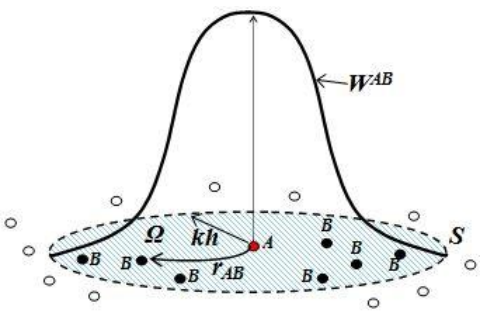

Fig. 1 SPH particle approximations in a three-dimensional problem domain Ω with a surface *S*. W^{AB} is the smoothing or kernel function that is used to approximate the field variables at particle *A* using averaged summations over particles *B* within the support domain, *κh*

Fig. 1 shows the problem domain consists of the discretization of body by particle, where each particle is associated with some field properties. These particles can be employed not only for integration, interpolation, and differentiation, but also for representing the material as mass particles. One may regard these particles as the mass centre of the corresponding sub-domains of the material. The volume of a sub-domain is lumped on the corresponding particle. Therefore, each particle is associated with a fixed lumped volume. We associate with particle *B* a volume, *dv*, to present the concept of particle mass, *m*

$$dv^B = \frac{m^B}{\rho^B} \tag{2}$$

where ρ^B is the density of particle *B*. Assuming that the kernel function has a compact supporting radius of *kh* and substituting Eq. (2) into (1), an approximation form of Eq. (1) by the discretized particles becomes

$$f(x^A) = \sum_{B=1}^{N} \frac{m^B}{\rho^B} f(x^B) W^{AB}(x^A - x^B, h) \tag{3}$$

where the summation is over all the particles (with a total number of *N*, including particle *A*) within the supporting domain of the given particle *A*. These influenced particles are the neighboring particles of particle *A*. The particle *B* has mass, m^B, position, x^B, density, ρ^B, velocity, v^B and other properties.

In this study, the B-spline function as shown in Fig. 2 is employed for the kernel function as shown in Eq. (4) to acquire a stable condition of the calculation.

$$W(q,h) = \frac{1}{h} \begin{cases} \frac{2}{3} - q^2 + \frac{1}{2}q^3 & 0 \le q < 1 \\ \frac{1}{6}(2-q)^3 & 1 \le q < 2 \\ 0 & q \ge 2 \end{cases} \tag{4}$$

where *q* is the distance between two particles *A* and *B*.

Finally, the function of particle *A* is calculated by using the first-order partial differentiation of kernel functions to solve Eq. (4). The first-order differentiation is only applied to the smoothing kernel function as shown in Eq. (5).

$$\nabla . f(x^A) = \sum_{B=1}^{N} \frac{m^B}{\rho^B} f(x^B) . \nabla W^{AB}(x^A - x^B, h) \tag{5}$$

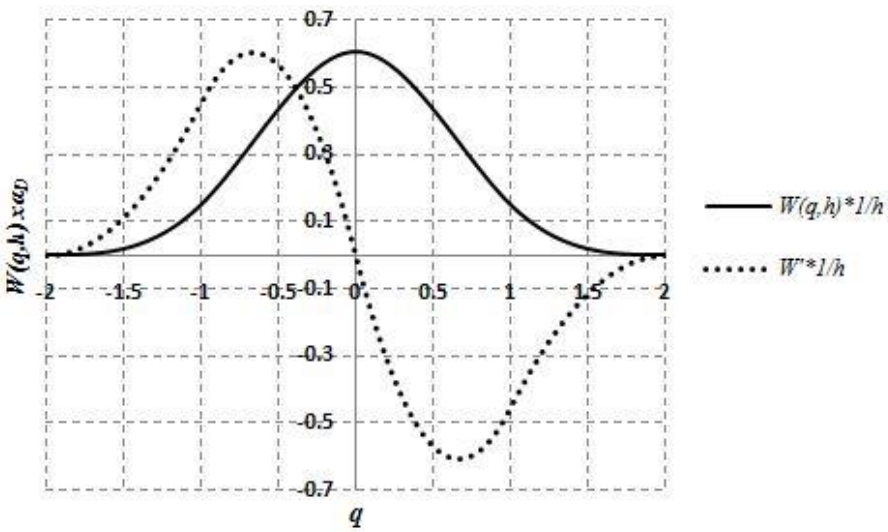

Fig. 2 The smoothing function, *W*, and its first derivative *W'*

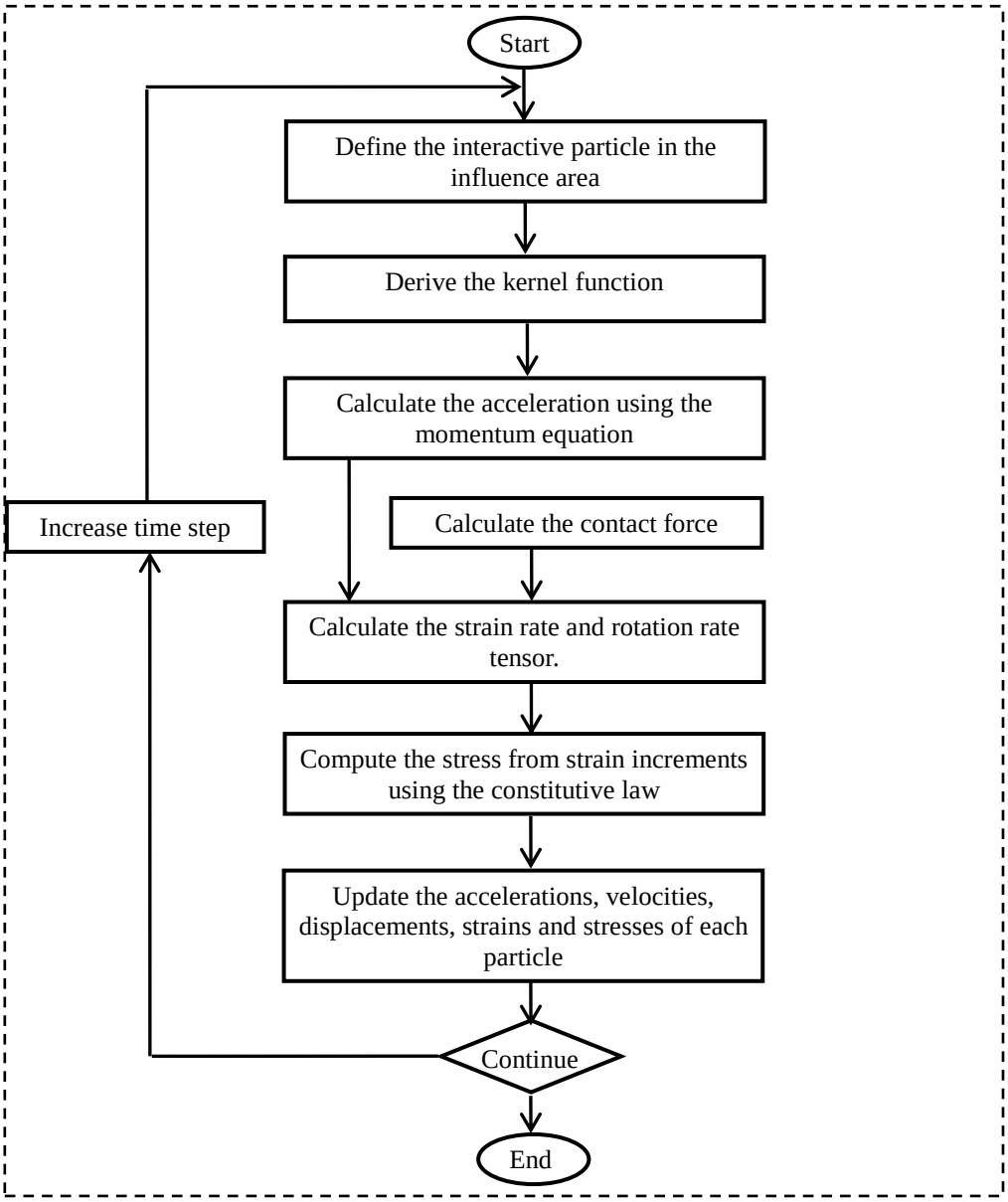

Fig. 3 Structure of calculation flow for the updated Lagrangian elastic-plastic analysis using SPH

It should be noted that the SPH particle approximations as explained above are employed to the governing equations such as the conservation of momentum equation to derive the motion of particles. The artificial viscosity of Monaghan (1985) is used to prevent immoderate penetration between particles during the impact response and aimed to smooth shocks over a few resolution lengths and to stabilize numerical solutions. Since this paper focused on the development of modified Drucker-Prager model, the derivation of discrete equations of motion in the SPH form and formulation of artificial viscocity used in this paper can be referred comprehensively in the

textbook and research thesis written by Liu and Liu (2003), Mokhatar (2013), respectively.

3.1 Calculation scheme of SPH for the analysis

The calculation scheme employed in this study for the updated Lagrangian elastic-plastic analysis is shown in Fig. 3 and described as follows:

(1) The interactive particles in the influence areas are defined prior at a every time increment where a certain number of particles within the support domain are used in the particle approximations.

(2) The derivative of kernel function as shown in Eq. (4) is calculated using the first-order partial differentiation as given in Eq. (5).

(3) The acceleration of particle *A* is computed under the force thread using the momentum equ ation. In the case of impact analysis, contact forces are calculated from the simple relationship between crossover volume and crossover area. The acceleration, velocity and displacement of each particle are then updated accordingly.

(4) Computation of the strain rate tensor and rotation rate tensor. Strain rate tensor and rotation can be written by the derivatives of the velocity as comprehensively explained by Liu and Liu (2003), Mokhatar (2013).

(5) The plasticity theory for yield criterion, the flow rule and the hardening rule of both concrete and steel materials are calculated under the stress thread. Explanation of this calculation is described in the following section.

(6) Then, the strain and stress are updated at every time step by time integration of strain ra te and by applying constitutive equation, respectively.

4. The material model

Next we present our adopted simple and reliable non-linear numerical method as well as the constitutive models of failure for concrete. Three basic schemes to present the localized failure of RC beam subjected to low velocity impact load are: (i) linear pressure-sensitive yield surface, in which DP with volume dependent PC hardening function when confining pressure occurs between 60 MPa~150 MPa are utilized (ii) two damage variables, tensile and compressive, are used to model different damaging behavior of concrete. Furthermore, strain softening in tension and compression is implemented during the post-peak regime by damage parameter to degrade the material stiffness (iii) two kinds of constitutive equations are developed to simulate the crushing, shear and bending cracking. All of these features are incorporated in the SPH method.

4.1 Yield function

The determination of plastic yielding and the control of the plastic volumetric change of concrete material are performed using the linear DP criterion with PC surface under confining pressure. Initially, the yield surface/failure line of this pressure-dependent (DP) model depends on two parameters; the slope of the failure line, α, and the intercept of the failure line, k, as displayed in Fig. 4.

In Fig. 4, x-axis represents the first invariant of stress tensor as shown in Eq. (6b). Meanwhile, the second invariant of deviatoric stress tensor forms the y-axis.

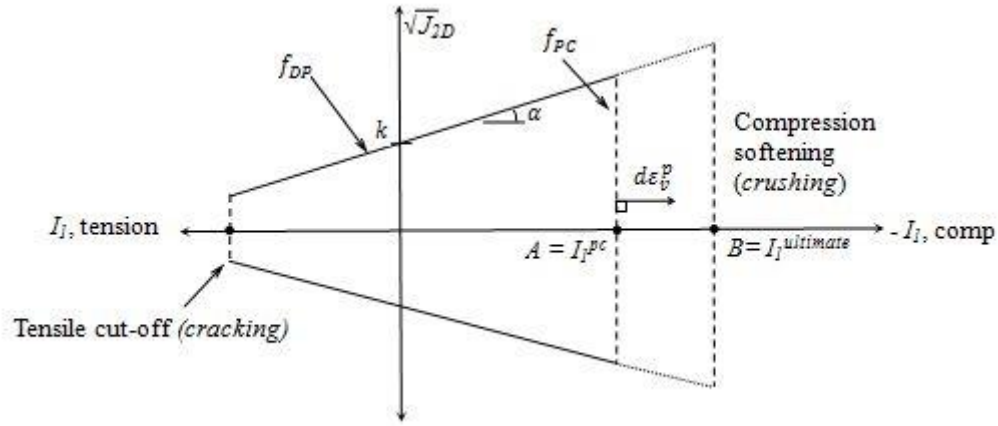

Fig. 4 Envelope for yield model of DP with PC surface

The generalized equation for the DP criterion by utilizing first invariant of stress tensor, I_1, and second invariant of deviatoric stress tensor, J_{2D}, is

$$f_{DP}(I_1, J_{2D}) = \sqrt{J_{2D}} + \alpha I_1 - k = 0, \qquad \sigma_t \le I_1^{pc} \le I_1^{ultimate} \tag{6a}$$

where

$$I_1 = \sigma_{11} + \sigma_{22} + \sigma_{33} = \sigma_{ij}\delta_{ij} \tag{6b}$$

$$\alpha = \frac{(\sigma_c - \sigma_t)}{\sqrt{3}(\sigma_c + \sigma_t)} \quad \text{and} \quad k = \left[\alpha + \frac{1}{\sqrt{3}}\right]\sigma_t \tag{6c}$$

In the equation above, α and k are the positive constants of the concrete material, while σ_{ij} is stress tensor. These constants can be related to the yield stress of compressive, σ_c and tensile, σ_t. Then, its elasto-plastic stiffness matrix has the following form

$$[D]^p = \begin{bmatrix} \frac{(H_1+H_2\sigma'_{11})^2}{H_3} & \frac{(H_1+H_2\sigma'_{11})(H_1+H_2\sigma'_{22})}{H_3} & \frac{(H_1+H_2\sigma'_{11})(H_1+H_2\sigma'_{33})}{H_3} & \frac{(H_1+H_2\sigma'_{11})(H_2\sigma'_{12})}{H_3} & \frac{(H_1+H_2\sigma'_{11})(H_2\sigma'_{13})}{H_3} & \frac{(H_1+H_2\sigma'_{11})(H_2\sigma'_{23})}{H_3} \\ & \frac{(H_1+H_2\sigma'_{22})^2}{H_3} & \frac{(H_1+H_2\sigma'_{22})(H_1+H_2\sigma'_{33})}{H_3} & \frac{(H_1+H_2\sigma'_{22})(H_2\sigma'_{12})}{H_3} & \frac{(H_1+H_2\sigma'_{22})(H_2\sigma'_{13})}{H_3} & \frac{(H_1+H_2\sigma'_{22})(H_2\sigma'_{23})}{H_3} \\ & & \frac{(H_1+H_2\sigma'_{33})^2}{H_3} & \frac{(H_1+H_2\sigma'_{33})(H_2\sigma'_{12})}{H_3} & \frac{(H_1+H_2\sigma'_{33})(H_2\sigma'_{13})}{H_3} & \frac{(H_1+H_2\sigma'_{33})(H_2\sigma'_{23})}{H_3} \\ & \text{Symmetry} & & \frac{(H_2\sigma'_{12})^2}{H_3} & \frac{(H_2\sigma'_{12})(H_2\sigma'_{13})}{H_3} & \frac{(H_2\sigma'_{12})(H_2\sigma'_{23})}{H_3} \\ & & & & \frac{(H_2\sigma'_{13})^2}{H_3} & \frac{(H_2\sigma'_{13})(H_2\sigma'_{23})}{H_3} \\ & & & & & \frac{(H_2\sigma'_{23})^2}{H_3} \end{bmatrix} \tag{7a}$$

where

$$H_1 = \alpha\left[3\lambda\delta_{kl} + 2\mu\delta_{kl}\right] \tag{7b}$$

$$H_2 = \frac{\mu}{\sqrt{J_{2D}}} \tag{7c}$$

$$H_3 = 3\alpha^2(3\lambda + 2\mu) + \mu + \left(\frac{2}{3}\right)\sqrt{J_{2D}}\,H\left[\alpha + \frac{1}{\sqrt{3}}\right] \quad H = \text{hardening modulus} \tag{7d}$$

The denotation σ'_{ij} is the deviatoric stress and μ and λ are the Lamè constants.

4.2 Compressive failure

The original DP yield surface gives large shear strength with large compressive confining pressure and there is no limiting bounds in the compression region. In the highly compressible conditions, certain compression limit is necessary to evaluate an accurate behavior of concrete material. Besides, the cap surface can be utilized to simulate the compressive failure under large mean stress. In this study, the PC surface is utilized to control the volumetric expansion as well as to displace the failure surface in the hydrostatic compression axis using the hardening rule. The cap criterion in the compressive side is defined by the compression cut-off. This is crucial for practical modeling of the volumetric expansion (dilatancy) under compression for frictional materials such as concrete.

Poinard *et al*. (2010) have conducted hydrostatic test for concrete under a very high-stress state. When the hydrostatic compression rises beyond 60 MPa, the cement matrix starts to damage and the behavior of concrete becomes cohesive-brittle, the property of which is governed by the crushing failure in the compression region. Thus, the initial compression failure surface I_1^{pc} at 60 MPa is adopted in order to control the plastic volumetric response. In this analysis, the limit (compression cut-off) for stress state is approximately twice or thrice the size of the concrete compressive strength, depending on its yield strength values. This limit is chosen in order to attain the possible cement-matrix-damage range. The yield criterion for PC is customarily represented as

$$f_{PC}(I_1, J_{2D}, I_1^{pc}(\varepsilon_v^p)) = I_1 - I_1^{pc}\left(\varepsilon_v^p\right) = 0, \qquad I_1 \geq I_1^{pc} \tag{8}$$

Generally, the concrete/mortar material fails in crushing such that some compression shearing cracks appear under compaction (impact region). By modifying the DP model, the cap can move outward due to proposed hardening rule during the plastic loading under volumetric compression stress state. Therefore, compaction can be predicted during loading and unloading in this state. This compaction leads to the plastic volumetric change in the hydrostatic compression.

The hardening rule of PC model is illustrated in Fig. 5, in which the hardening mechanism is expressed by the relationship between plastic volumetric strain, ε_v^p, and the first stress invariant, I_1, as given in Eq. (9a)

$$I_1^{pc}(\varepsilon_v^p) = \left[\frac{h'}{\left(1 + e^{\varepsilon_v^p}\right)}\right] \tag{9a}$$

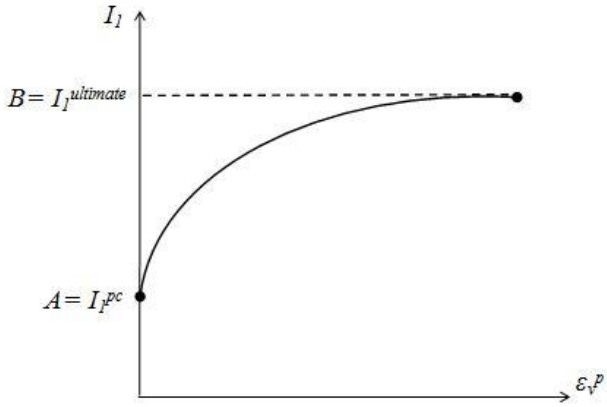

Fig. 5 Nonlinear hardening rule

where

$$h' = 2.5\sigma_c \tag{9b}$$

$$\varepsilon_v^p = \varepsilon_{11}^p + \varepsilon_{22}^p + \varepsilon_{33}^p = \varepsilon_{ij}^p \delta_{ij} \tag{9c}$$

The value of the first invariant of stress tensor and volumetric plastic strain are always negative (since negative sign means compression state).

4.2.1 Plane Cap (PC) model

The constitutive equation for PC model is now derived. Substitute Eq. (9a) into Eq. (8) to express the function of the PC model

$$f_{PC} = I_1 - \frac{h'}{\left(1 + e^{\varepsilon_v^p}\right)} \tag{10}$$

The general form of a plastic multiplier can be obtained as

$$\lambda_{pc} = \frac{\dfrac{\partial f}{\partial \sigma_{ij}} D_{ijkl}^e d\varepsilon_{kl}}{\dfrac{\partial f}{\partial \sigma_{ab}} D_{abmn}^e \dfrac{\partial f}{\partial \sigma_{mn}} - \dfrac{\partial f}{\partial \varepsilon_{ij}^p} \dfrac{\partial f}{\partial \sigma_{ij}}} \tag{11}$$

Differentiating Eq. (10) and substituting the derivatives as well as the fourth-order tensor of elastic stiffness, $D_{ijkl}^e = \lambda(\delta_{ij}\delta_{kl}) + \mu(\delta_{ik}\delta_{jl} + \delta_{il}\delta_{jk})$ into Eq. (11), the plastic multiplier of the cap is defined by

$$\lambda_{pc} = \frac{[3\lambda + 2\mu] d\varepsilon_{mm}}{[9\lambda + 6\mu] + \dfrac{3h' e^{\varepsilon_v^p}}{\left(1 + e^{\varepsilon_v^p}\right)^2}} \tag{12}$$

Finally, by applying the Einstein summation rule the constitutive equation of the plane cap takes the following form

$$d\sigma_{ij} = \left[D^{e}_{ijkl} - \frac{[3\lambda + 2\mu]\delta_{ij}[3\lambda + 2\mu]\delta_{kl}}{[9\lambda + 6\mu] + \dfrac{3h' e^{\varepsilon_v^p}}{\left(1 + e^{\varepsilon_v^p}\right)^2}} \right] \delta_{mk}\delta_{nl} d\varepsilon_{kl} \tag{13}$$

where the plastic stiffness matrix is written in Eq. (14).

$$[D]^{ep}_{PC} = \begin{bmatrix} (\lambda+2\mu) - \dfrac{(3\lambda+2\mu)^2}{(9\lambda+2\mu) + \dfrac{3h' e^{\varepsilon_v^p}}{\left(1+e^{\varepsilon_v^p}\right)^2}} & \lambda - \dfrac{(3\lambda+2\mu)^2}{(9\lambda+2\mu) + \dfrac{3h' e^{\varepsilon_v^p}}{\left(1+e^{\varepsilon_v^p}\right)^2}} & \lambda - \dfrac{(3\lambda+2\mu)^2}{(9\lambda+2\mu) + \dfrac{3h' e^{\varepsilon_v^p}}{\left(1+e^{\varepsilon_v^p}\right)^2}} & 0 & 0 & 0 \\ & (\lambda+2\mu) - \dfrac{(3\lambda+2\mu)^2}{(9\lambda+2\mu) + \dfrac{3h' e^{\varepsilon_v^p}}{\left(1+e^{\varepsilon_v^p}\right)^2}} & \lambda - \dfrac{(3\lambda+2\mu)^2}{(9\lambda+2\mu) + \dfrac{3h' e^{\varepsilon_v^p}}{\left(1+e^{\varepsilon_v^p}\right)^2}} & 0 & 0 & 0 \\ & & (\lambda+2\mu) - \dfrac{(3\lambda+2\mu)^2}{(9\lambda+2\mu) + \dfrac{3h' e^{\varepsilon_v^p}}{\left(1+e^{\varepsilon_v^p}\right)^2}} & 0 & 0 & 0 \\ & \text{Symmetry} & & 2\mu & 0 & 0 \\ & & & & 2\mu & 0 \\ & & & & & 2\mu \end{bmatrix} \tag{14}$$

The above constitutive equation for material loading conditions are employed when the stress state reaches the point *A* as shown in Fig. 4. After this point, the increment of stress as derived in Eq. (13) produces volume change by the movement of the cap surface.

4.2.2 Nonlinear strain softening

Generally, the concrete material fails in crushing. If the materials has crushed in compression, it is assumed that there occurs also the strain softening. In this analysis, when the state of stress exceeds a certain critical value, concrete will fail by crushing. At this point, all stress components are released homogeneously and the material is assumed to lose its strength entirely against any type of further deformation (see Fig. 6).

The degradations of material stiffness correspond to the same damage parameter such that they are expressed by the integrity tensor, φ

$$\varphi^2 = (1 - D) \tag{15}$$

where the scalar degradation (damage), *D*, is caused by the confining pressure defined as a volumetric plastic strain

$$D = f(\varepsilon_v^p) = \frac{\left(\varepsilon_v^p\right)^2}{\varepsilon_{cru}} \tag{16}$$

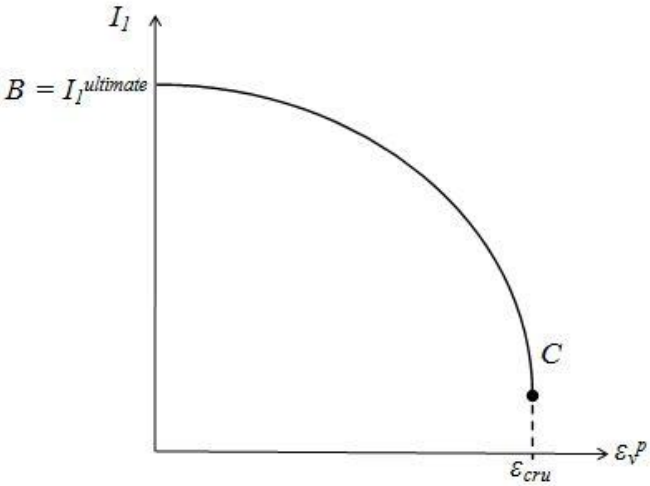

Fig. 6 Nonlinear softening rule

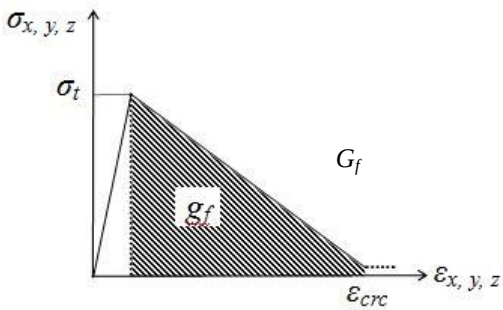

Fig. 7 Strain-softening in tension

When the parameter ε_v^p reaches the crushing strain limit, ε_{cru}, it is assumed that the damage parameter, φ, becomes almost zero. The crushing strain limit is assumed by the simple equation

$$\varepsilon_{cru} = \frac{E}{\sigma_c} \times \frac{1}{10000} \tag{17}$$

where E is the Young's modulus of concrete. Finally, the form of constitutive equation after point B can be expressed by the multiplication of Eq. (15) with (14) as below

$$\{d\sigma_{ij}\} = \left[D_{ijkl}^{ep}\right] \times \varphi^2 \{d\varepsilon_{kl}\} \tag{18}$$

4.3 Tensile failure

In the tension region, the flexural and shear cracking are common prominent features of concrete failure mechanism. It has been known that this tensile cracking degrades the stiffness of concrete material. Thus, this paper considers the local material orthotropy caused by tensile failure of concrete, in which the failure initiates the decrease of elastic stiffness normal to the crack

direction isotropically. The plasticity and damage are directly defined after the tensile strength, σ_t, is exceeded using the softening path. The stiffness degradation of the concrete materials in tensile side can be identified by the linear tension-softening path as shown in Fig. 7. In addition, the ultimate strain, ε_{crc}, (end point of softening path) is assumed and its adequate value is chosen in order to prevent particle size dependency using the relation between fracture energy, G_f, and particle size.

Generally, we consider the mortar to be formed by fine aggregates having a maximum diameter of 2 mm. Thus, 50 N/m is chosen as the value of G_f due to the specific fracture energy of mortar. Besides, the particle size employed in this analysis is 5 mm.

The cracking of the material is assumed to propogate in the direction normal to the principal tensile strain. The integrity tensor, φ_i^+ ($i = x,y,z$) is introduced in the tensile side by considering the positive values of principle strain; in which the principal value and its direction are calculated by the eigenvalue analysis based on each of the strain on target particle.

$$\left(\varphi_x^+\right)^2 = \left(1 - d_x\right), \quad \therefore \left(d_x = \frac{\varepsilon_x^+}{\varepsilon_{crc}}\right) \tag{19a}$$

$$\left(\varphi_y^+\right)^2 = \left(1 - d_y\right), \quad \therefore \left(d_y = \frac{\varepsilon_y^+}{\varepsilon_{crc}}\right) \tag{19b}$$

$$\left(\varphi_z^+\right)^2 = \left(1 - d_z\right), \quad \therefore \left(d_z = \frac{\varepsilon_z^+}{\varepsilon_{crc}}\right) \tag{19c}$$

Then, the damage formulations according to Eq. (19) are multiplied with the initial fourth-order isotropic elastic matrix. Finally, the orthotropic constitutive equation and its stiffness matrix can be formed as shown in Eqs. (20) and (21), respectively.

$$\sigma_{ij} = \varphi_x^+ \varphi_y^+ \varphi_z^+ \left[D_{ijkl}^e\right] \varepsilon_{kl} \tag{20}$$

$$[D]^e = \begin{bmatrix} \varphi_x^2(\lambda + 2\mu) & \varphi_x\varphi_y\lambda & \varphi_x\varphi_z\lambda & 0 & 0 & 0 \\ & \varphi_y^2(\lambda + 2\mu) & \varphi_y\varphi_z\lambda & 0 & 0 & 0 \\ & & \varphi_z^2(\lambda + 2\mu) & 0 & 0 & 0 \\ & & & \varphi_x\varphi_y 2\mu & 0 & 0 \\ & \text{Symmetry} & & & \varphi_y\varphi_z 2\mu & 0 \\ & & & & & \varphi_z\varphi_x 2\mu \end{bmatrix} \tag{21}$$

5. Analysis and results discussion

The proposed model is implemented in the JAVA code program incorporated with the SPH method and is verified with two experimental results conducted elsewhere. For convenience, we numerically explore in the current study the impact tests carried out by Kishi *et al*. (2003) and Sonoda *et al*. (2012) concerning the high mass-low velocity impact behavior of reinforced concrete beam. In order to distinguish the impact tests and its failure mode, the denotations as in Table 1 are employed.

Table 1 Denotation of specimen and its failure characteristic

Specimen	Span (mm)	Velocity (m/s)	Failure characteristic	Literature
K2000-4.4	2000	4.4	Bending cracks at the centre of the bottom part of concrete and cracks propagate along the lower region of specimen.	Kishi *et al*. (2003)
S800-3.5	800	3.5	Flexural and shear cracks, total crush on the impact region.	Sonoda *et al.* (2012)

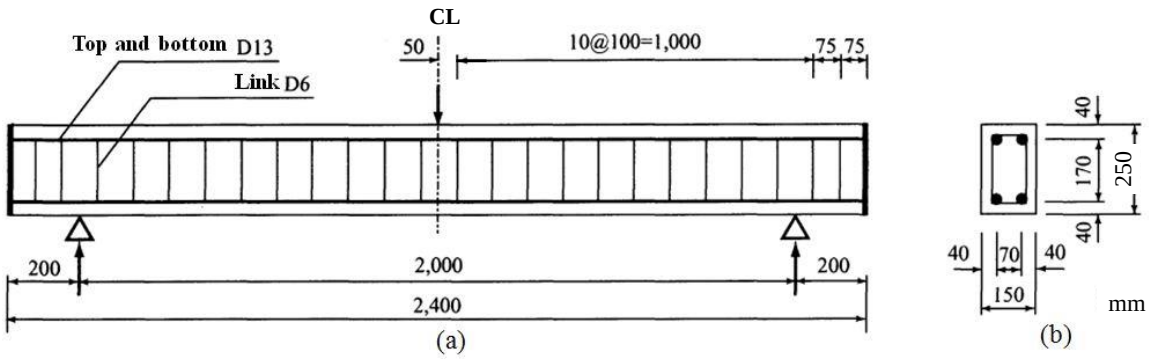

Fig. 8 Rebar arrangement (a) side view (b) cross-sectional view

Table 2 Concrete and steel reinforcement properties

Properties \ Material	Concrete	Steel
Young Modulus (N/m^2)	2.050×10^{10}	2.020×10^{11}
Poisson's ratio	0.17	0.3
Density (kg/m^3)	2350	7850
Compressive yield Stress, σ_c (N/m^2)	31.68×10^6	366×10^6
Tensile yield stress, σ_t (N/m^2)	3.16×10^6	366×10^6

5.1 K2000-4.4

Kishi *et al*. (2003) presented different impact experiments of RC beams under a variety of velocities. A RC beam with details as described in Fig. 8 with a length of 2400 mm is chosen to validate the proposed numerical analysis. They used a 300 kg steel drop-weight, which was impacted onto a beam, and the related properties of material are presented in a tabulated form as shown in Table 2.

We adopt simply-supported models with a length half that of experiment with 10 mm particle size for the numerical simulation in order to simplify the analysis. All analyses in this paper assume a perfect bonding interaction between concrete and steel reinforcement. The crack patterns formed after the 4.4 m/s impact velocity is shown in Fig. 9 (a). In the experimental tests, it can be seen that many vertical cracks are developed from the lower edge of the beam,which then propagate to the loading point, and no severe shear cracks are observed. This phenomenon has been replicated numerically (see Fig. 9 (b)) by using pressure-volume dependent and softening

technique as explained in the preceding Sections 4.1, 4.2 and 4.3. The distribution of cracks are demonstrated when the positive stress state exceeds the tensile strength. The principal strain is extracted from the six components of strain values and defined as the tension damage parameter. The cracking is considered when the maximum principal strain value, ε_{kk}^{max}, is more than 5000μ and 10000μ. From the modeled results, it can be seen that the RC beam is completely cracked vertically, which matches well with experiment.

The integration of Drucker-Prager with a simple plane cap surface (DPPC) that is used in the high-stress state area can simulate the compression response satisfactorily. As stated in the preceding section, the cap model (see Fig. 4) has some desirable features. Based on the analysis results, it can be noted that by applying the PC constitutive equation in Eqs. (13) and (14) for the compression side, the crushing phenomenon can be simulated accurately beneath the impact area (see Fig. 9 (b)). However, the application of DPPC criteria shows an instability in rebar particles, which results in an impractical fracture. Thus, this study utilizes the average velocity, $\hat{v}$, for the rebar particle as proposed by Gray *et al.* (2001) in order to keep the movement of particles in an orderly manner. The average velocity differs from the actual velocity, where v^A is replaced by $\hat{v}^A$ as given in Eq. (22).

$$\hat{v}^A = v^A + \psi \sum_B \frac{m^B}{\rho^B}\left(v_i^A - v_i^B\right) W^{AB} \tag{22}$$

The value of 0.3 is chosen for the constant parameter, ψ, in order to simulate the RC beam with no sign of unrealistic particle separation in rebar. Although the numerical instability in tension rebar cannot be fixed completely by using the average velocity, the degree of particle separation is reduced to a satisfactory condition as shown in Fig. 9(c). For further comparison, the computed impact force-time histories can be seen in Fig. 10. Based on these curves, it can be observed that the maximum mid-span displacement by utilizing the average velocity is smaller than that of experimental results. Additionally, the residual displacement gives a 15 mm difference compared to the experimental results. It is interesting to notice that moving the particle with the average velocity, $\hat{v}$, affects the displacement calculations.

A number of researchers such as Colin *et al.* (1995), Nandlall and Wong (1999), Beppu *et al.* (2008), Luccioni and Aráoz (2011) have employed an erosion algorithm incorporated with FEM and SPH to allow the simulation of material fracture, perforation and penetration. In general, a number of mechanisms are available to initiate the erosion of elements or particles and this can be used in any combination. Elements and particles will erode if any of the criteria are met. An instantaneous geometric strain is employed in this analysis as a numerical erosion criterion and its ultimate value is assumed to be 100μ. A value of 100μ is chosen as the specified limit $(\varepsilon_{eff})_{\lim}$ due to small value of strain components that is used in the quadratic form of the effective strain equation. This erosion criteria allows decreasing the influence area (support domain) when the instantaneous geometric strain exceeds $(\varepsilon_{eff})_{\lim}$. After this point, the particle connectivity has been disintegrated by means of decreasing of influence domain.

$$\varepsilon_{eff} = \frac{2}{3}\sqrt{\left[\left(\varepsilon_{11}^2 + \varepsilon_{22}^2 + \varepsilon_{33}^2\right) + 5\left(\varepsilon_{11}\varepsilon_{22} + \varepsilon_{22}\varepsilon_{33} + \varepsilon_{33}\varepsilon_{11}\right) + 3\left(\varepsilon_{12}^2 + \varepsilon_{23}^2 + \varepsilon_{31}^2\right)\right]} \geq (\varepsilon_{eff})_{\lim} \tag{23}$$

Applying the concept of decreasing the influence area when the instantaneous geometric strain exceeds the effective strain limit by means of erosion criteria, the numerical results as in Fig. 9 (d) provide a sensibly accurate failure mode in terms of crushing and bending cracks. It is also found that the erosion algorithm contributes to a reasonable maximum displacement value and the shape

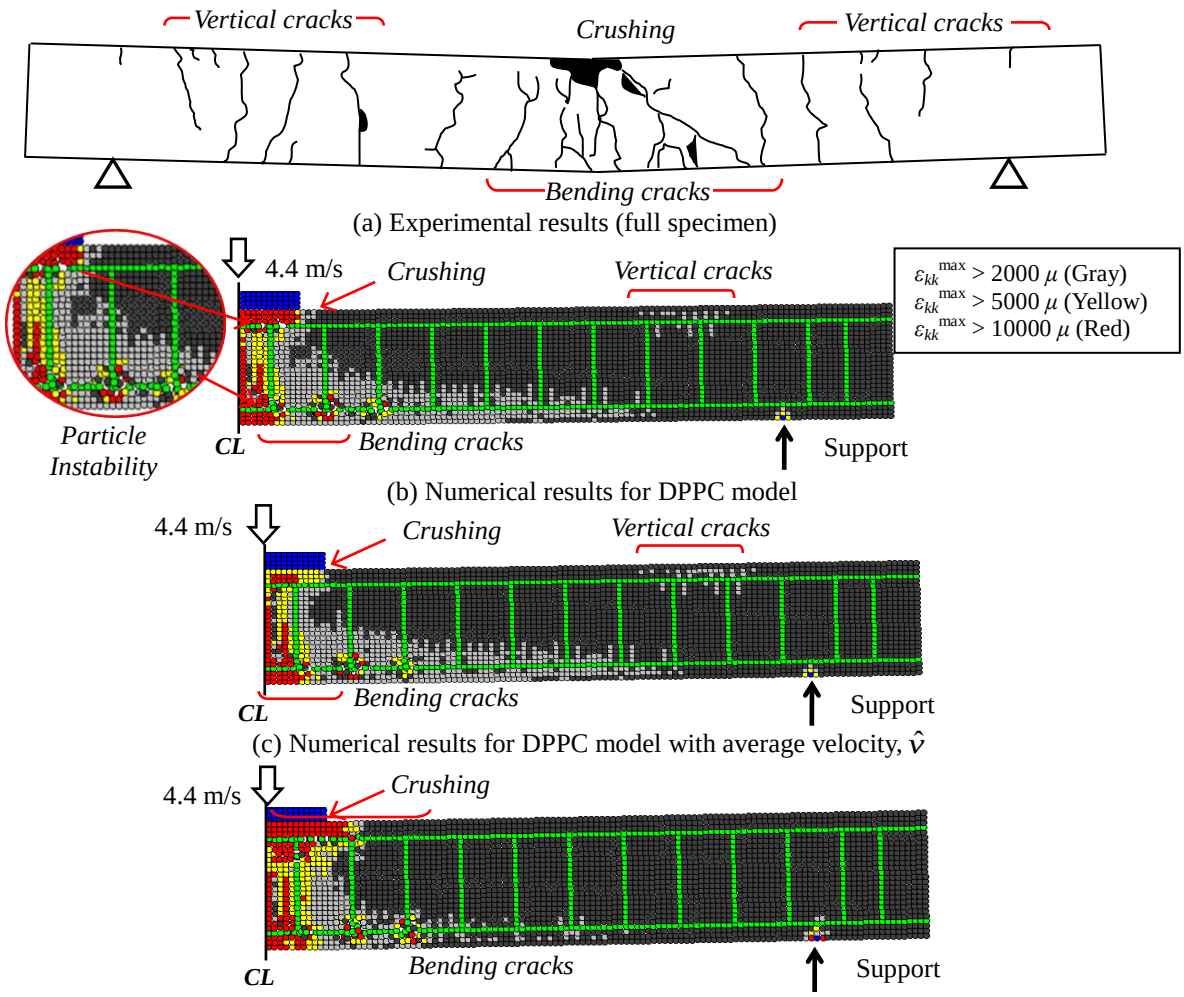

(a) Experimental results (full specimen)

(b) Numerical results for DPPC model

(c) Numerical results for DPPC model with average velocity, $\hat{v}$

(d) Numerical results for DPPC model with average velocity, $\hat{v}$ and erosion criteria

Fig. 9 Comparison of numerical and experimental results for K2000-4.4 specimen

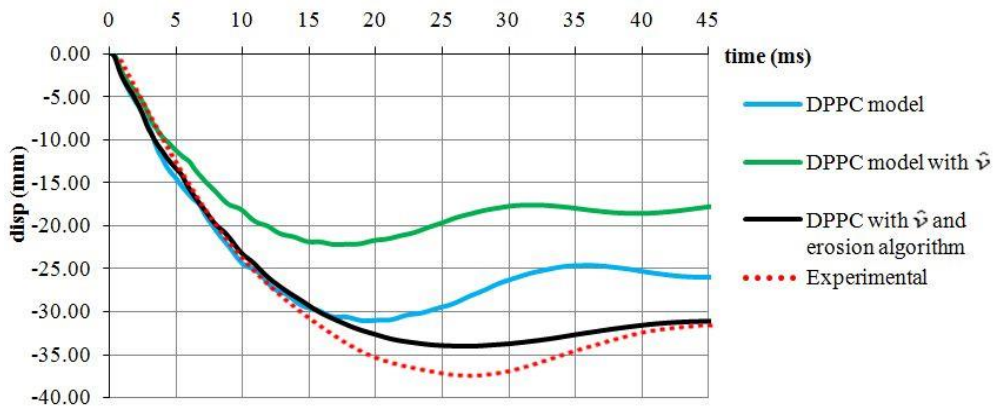

Fig. 10 Displacement-time histories for K2000-4.4 specimen

of the displacement curve is comparatively the same as compared to the experimental results (refer Fig. 10).

5.2 S800-3.5

The crushing and flexural failure mechanisms of the S800-3.5 specimen from the experimental work of Sonoda *et al.* (2012) are the highlights of this investigation to verify the ability of the proposed model. The related specimen details and material properties are given as in Fig. 11 and Table 3. The numerical simulation is conducted using a quarter size of that studied by Sonoda *et al.* (2012) by applying symmetry condition, with 5 mm particle size and 900 mm length.

The experimental result (refer Fig. 12 (a)) shows the predominant crushing occurs beneath the impact zone, and the flexural failure propagates from the bottom of the beam towards the top region. Further shear cracking and short vertical crack as well as yielding of the tension rebar occur in the beam specimen. Since the aim is to focus only on mortar beam failure simulation, the yielding of steel reinforcement is not discussed in this study. Based on the experimental results, there is an extensive crushing in the impact region, due to the proportionally more significant amount of energy in the crushing area.

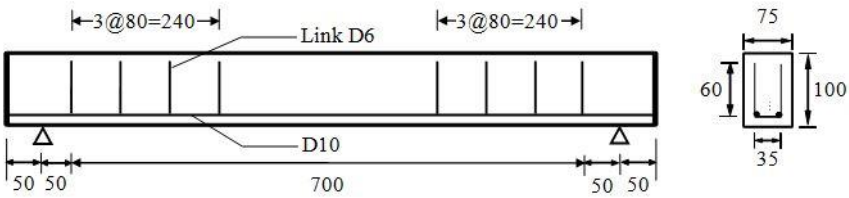

Fig. 11 Rebar arrangement (a) side view (b) cross-sectional view

Table 3 Mortar and steel reinforcement properties

Properties \ Material	Mortar	Steel
Young Modulus (N/m^2)	1.66×10^{10}	2.06×10^{11}
Poisson's ratio	0.22	0.3
Density (kg/m^3)	2400	7800
Compressive yield Stress, σ_c (N/m^2)	23.78×10^6	300×10^6
Tensile yield stress, σ_t (N/m^2)	2.37×10^6	300×10^6

The proposed failure criterion is decomposed into two components, deviatoric and volumetric plastic strains, as readily illustrated in Section 4.1, where the volumetric plastic strain changes during the cap yielding. However, this study employs the plane cap surface, in which during the movement of the cap, there is no change of deviatoric plastic strains. Thus, the prediction of shear cracks is unable to be observed clearly in Fig. 12 (b), (c) and (d). In the numerical results, the failure in maximum deformed condition is indicated when the maximum principal strain value, ε_{kk}^{max}, exceeds 4000μ, 8000μ and 11000μ. The degree of compaction in the compressed region is controlled by the hardening rule of the DPPC model. Although this model is able to simulate the

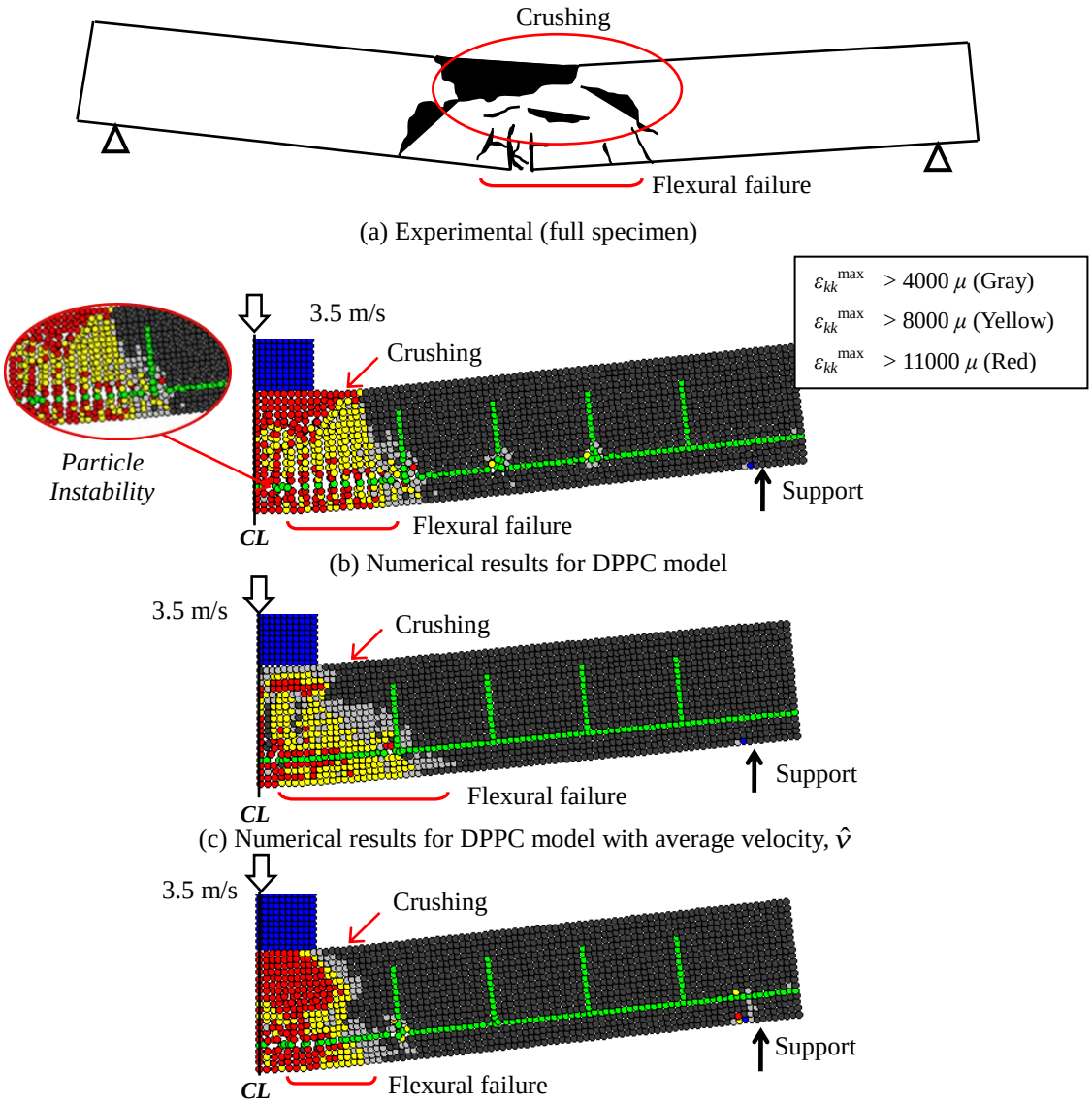

(d) Numerical results for DPPC model with average velocity, $\hat{v}$, and erosion criteria

Fig. 12 Comparison of numerical and experimental results for S800-3.5 specimen

crushing phenomena adequately as revealed in Fig. 12 (b), the particle in the tension area especially the rebar particles show a great deal of dispersion. In Fig. 12 (c), the numerical simulations are shown at the same time increment as in Fig. 12 (b), but the analysis is calculated using the average velocity with an appropriate constant value 0.3. As a result, the particle instability in tension region disappear.

Focusing and examining the impacted regions, it is interesting to see that the DPPC model incorporated with the average velocity and erosion criteria as shown in Fig. 12 (d) exhibits reasonably close resemblance to that demonstrated by the experimental work. Particularly of

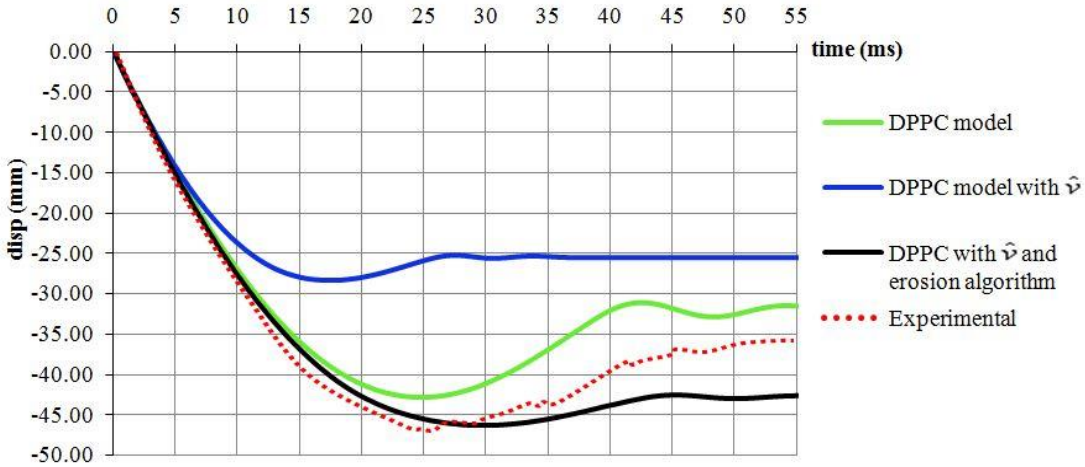

Fig. 13 Displacement-time histories for S800-3.5

interest are the high compression stress states, in which a larger area of crushing appears and covers the impact zone. It is important to note that the combination of average velocity and erosion algorithm are able to express the impact failure with considerably good agreement with the experimental results in terms of compressive failure.

The comparisons of displacement-time relationship between the numerical analysis and experimental results can be seen in Fig. 13. It is confirmed that by including the average velocity and erosion criteria in the numerical simulation, the computed maximum displacement conforms practically to that of experimental work. It should also be noted that the simulation without considering the average velocity and erosion algorithm gives a reasonably well replication of displacement curve and maximum values as indicated by the black colour curve. The effect of model with average velocity but without erosion algorithm decreases the maximum displacement approximately 30 percent of that with erosion. Even though the model with average velocity but no erosion algorithm displays differences in the displacement profile, it reduces the fragmentation of particle in tension regions satisfactorily.

6. Conclusions

This paper investigates the impact response of RC beam by means of the SPH approach by modifying the DP criterion incorporating the PC with a lesser parameter identification of hardening rule in the compression zone. The yielding of concrete using the PC model in compression zone and the fracture property in tension zone are combined, where the PC model in the tensile area is employed associating with the linear softening. This approach consists of linear and nonlinear softening in tension and compression regions, respectively, to express the complex behaviour of concrete and mortar material during a short time loading condition. The model is a combination of the generalized effective space plasticity theory followed by the damage theory applied simultaneously under the assumptions of small strain. In order to simulate the compression failure under high stress state, the erosion criteria associated with the decreasing of an influence domain in this zone has been proved to be a useful tool to provide a sensibly accurate result. The

erosion criteria allow decrease of the influence area (support domain) when the instantaneous geometric strain exceeds the effective strain limit such that the particle connectivity is then disintegrated.

The simulated results match those experimental in terms of the crushing, flexural cracks and displacement especially when average velocity and erosion algorithm are incorporated. It should be noted that these results can be extrapolated to RC slabs simulation under high velocity impact loads. Further improvement of the model is required to enhance the numerical results in reproducing realistic estimation of damage behavior of RC elements when involving large deformation. Another future consideration involves the use of nonlinear envelope criterion with an optimum number of parameters.

References

Beppu, M., Miwa, K., Itoh, M., Katayama, M. and Ohno, T. (2008), "Damage evaluation of concrete plates by high-velocity impact", *Int. J. Impact Eng.*, **35**(12), 1419-1425.

Charles, E.A. (1987), "An overview of the theory of hydrocodes", *Int. J. Impact Eng.*, **5**(1-4), 33-59.

Chen, Y. and May, I.M. (2009), "Reinforced concrete members under drop-weight impacts", *Proceeding of the Institution of Civil Engineers*, **162**(1), 45-56.

Colin, J.H., Ranson, H.J., David, J.G. and Naury, K.B. (1995), "Modelling of microparticle hypervelocity oblique impacts on thick targets", *Int. J. Impact Eng.*, **17**(1-3), 375-386.

Faham. T. (2008), *Numerical modelling of reinforced concrete slabs subjected to impact loading*, Master Thesis, University of Wollongong, Australia.

Fujikake, K., Li, B. and Soeun, S. (2009), "Impact response of reinforced concrete beam and its analytical evaluation", *J. Struct. Eng*., ASCE., **135**(8), 938-950.

Fukazawa, J. and Sonoda, Y. (2011), "An accuracy of impact failure response of reinforced concrete beam using ASPH method", *J. Struct. Eng., Japan Soc. Civil Eng.*, **57A**, 1205-1212. (in Japanese)

Gang, L., Xibing, L. and Kejin, W. (2012), "A numerical study on the damage of projectile impact on concrete targets", *Comput Concrete*, **9**(1), 21-33.

Gray, J.P., Monaghan, J.J. and Swift, R.P. (2001), "SPH elastic dynamics", *Comp. Meth. App. Mech. Eng.*, **190**(49-50), 6641-6662.

Gulkan, P. and Korucu, H. (2011), "High-velocity impact of large caliber tungsten projectiles on ordinary Portland and calcium aluminate cement based HPSFRC and SIFCON slabs. Part II: numerical simulation and validation", *Struct. Eng. Mech*., **40**(5), 617-636.

Johnson, G.R. (2011), "Numerical algorithms and material models for high-velocity impact computations", *Int. J. Impact Eng.*, **38**(6), 456-472.

Kantar, E., Erdem, R.T. and Anil, O. (2011), "Nonlinear finite element analysis of impact behavior of concrete beam", *Math. Comp. Apps.*, **16**(1), 183-193.

Kishi, N., Ohno, T., Mikami, H. and Ando, T. (2003), "Effects of boundary conditions on impact behaviors of reinforced concrete beams subjected to falling-weight impact loads", *Proc. Japan Soc. Civil Eng.*, **731**(I-63), 299-316. (in Japanese)

Lavoie, M.A., Gakwaya, A. and Ensan, M.N. (2015), "Application of SPH method for simulation of aerospace structure under impact loading", *10th International LS-DYNA User Conference*, 35-42.

Liu, G.R. and Liu, M.B. (2003), *Smoothed Particle Hydrodynamics: A Meshfree Particle Method*, World Scientific Publishing Co. Pte. Ltd.

Liu, M.B., Liu, G.R. and Lam, K.Y. (2006), "Adaptive smoothed particle hydrodynamics for high strain hydrodynamics with material strength", *J. Shock Wav.*, **15**(1), 21-29.

Luccioni, B. and Aráoz, G. (2011), "Erosion criteria for frictional materials under blast load", *Mecánica Computacional*, **XXX**(21), 1809-1831.

Ma, S., Zhang, X. and Qiu, X.M. (2009), "Comparison study of MPM and SPH in modeling hypervelocity impacts problems", *Int. J. Impact Eng.*, **36**(2), 272-282.

Mokhatar, S.N. (2013), "Quantitative impact response analysis of reinforced concrete beam using the SPH method", Doctoral Thesis, Kyushu University, Japan.

Mokhatar, S.N., Abdullah, R. and Kueh, A.B.H. (2013), "Computational impact responses of reinforced concrete slabs", *Comput. Concrete*, **12**(1), 37-51.

Mokhatar, S.N., Sonoda, Y. and Jaini, Z.M. (2013), "Nonlinear simulation of beam elements subjected to high mass low velocity impact loading using the smoothed particle hydrodynamics (SPH) method", *Int. J. Integrat. Eng.*, **5**(2), 37-42.

Monaghan, J.J. and Lattanzio, J.C. (1985), "A refined particle method for astrophysical problems", *Astron. Astroph.*, **149**, 135-143.

Nandlall, D. and Wong, G. (1999), *A numerical analysis of the effect of erosion strain on ballistic performance prediction*, DREV-TM-1999-05, Unclassified.

Park, H. and Kim, J.Y. (2005), "Plasticity model using multiple failure criteria for concrete in compression", *Int. J. Solid. Struct.*, **42**(8), 2302-2322.

Poinard, C., Malecot, Y. and Daudeville, L. (2010), "Damage of concrete in very high stress state: experimental investigation", *Mater. Struct.*, **43**(1-2), 15-29.

Rabczuk, T. and Eibl, J. (2006), "Modelling dynamic failure of concrete with meshfree methods", *Int. J. Impact Eng.*, **32**(11), 1878-1897.

Saatci, S. and Vecchio, F.J. (2009), "Nonlinear finite element modeling of reinforced concrete structures under impact loads", *ACI Struct. J.*, **106**(5), 717-725.

Sangi, A.J., Khan, R.A. and May, I.M. (2010), "Behaviour of RC beams under multiple impact loads", *The First International Conference of Protective Structures*, Manchester, London, October.

Sonoda, Y., Mokhatar, S.N. and Tokumaru, S. (2012), "Elastic plastic impact response of beam element subjected to low velocity impact load using SPH method", *J. Appl. Mech.*, JSCE A2, **68**, 373-381.

Swaddiwudhipong, S., Islam, M.J. and Liu, Z.S. (2010), "High velocity penetration/perforation using coupled smoothed particle hydrodynamics-finite element method", *Int. J. Protect. Struct.*, **1**(4), 489-506.

Tokumaru, S., Sonoda, Y., Fukazawa, J. and Mokhatar, S.N. (2011), "A fundamental study on the impact failure mechanism of reinforced mortar beam using SPH method", *Proc. Japan Concrete Inst.*, **33**, 775-780. (in Japanese)

Unosson, M. (2009), "Numerical simulations of the response of reinforced concrete beams subjected to heavy drop tests", *Fourth Int. Symposium on Impact Eng.*, 613-618.

Youcai, W., Choi, H.J. and Crawford, J.E. (2013), "Concrete fragmentation modeling using coupled finite element-meshfree formulations", *Interact. Multis. Mech.*, **6**(2), 173-195.

Zhou, X.Q., Kuznetsov, V.A., Hao, H. and Waschl, J. (2008), "Numerical prediction of concrete slab response to blast loading", *Int. J. Impact Eng.*, **35**(10), 1186-1200.

PL

Nomenclature

h	influence area
A	particle A
B	particle B
dv	volume of the integral that contains all particles
Ω	domain integral
S	surface of support domain

$f(x^A)$	functions of target particle A
$f(x^B)$	function of neighboring particle B
W^{AB}	kernel function
W' and ∇W	first derivative of kernel function
q	relative distance between two point particles
N	number of particles in influence domain
δ_{ij}	Kronecker-delta
σ_{ij}	stress tensor
I_1	first invariant of stress tensor
I_1^{pc}	initial compression limit
$I_1^{ultimate}$	initiation point of post peak regime
σ_c	yield stress (compressive)
σ_t	yield stress (tensile)
J_{2D}	second invariant of deviatoric stress tensor
H	hardening modulus
E	Young's modulus
ε_v^p	volumetric plastic strain
λ_{pc}	plastic multiplier for plane-cap model
λ, μ	Lamè constants
G_f	fracture energy
ε_{crc}	cracking strain limit
ε_{cru}	crushing strain limit
φ	integrity tensor
D	scalar damage parameter
D^e_{ijkl}	initial elastic stiffness
$(\varepsilon_{eff})_{\lim}$	limit for the instantaneous geometric strain